An N-Point Linear Solver for Line and Motion Estimation with Event Cameras

Supplementary Material

7. Appendix

Here we report additional results of our algorithm for varying noise sources in Sec. 7.1, before discussing the proofs of Theorem 1 and Theorem 2 in Sec. 7.2 and Sec. 7.3, as well as the connection of our proposed line averaging scheme with that of [12] in Sec. 7.6. Finally, we provide additional visual insights into the manifolds spanned by events generated by a line. We show that these manifolds can be canonicalized, *i.e*. reduced to a small family of manifolds which are highly interpretable (see Sec. 7.7).

7.1. Noise Sensitivity Analysis

In Fig. 5, we provide additional results of our method in simulation, as we vary the number of events used by our solver, and the magnitude of the various noise sources, *e.g*. pixel noise, timestamp jitter, gyroscope noise. As expected, we see that all errors decrease as more events are used, and errors increase as more noise is injected. Again, the only noise source that cannot be completely eliminated through addition of events is the gyroscope noise, which introduces systematic errors. Experimentally, we found that $N = 10$ events gives a good tradeoff between the speed of the algorithm, and observed errors for all noise levels and sources.

We also present additional results for differing noise sources and magnitudes of our line averaging scheme in Fig. 6, and analyse the resulting errors as the number of used lines increases. Again we see that all errors tend to zero as more lines are used, except for the gyroscope noise.

7.2. Proof of Theorem 1 on Degeneracies

For clarity, we restate Theorem 1 here:

Theorem 1: *If rank*$(\mathbf{A}) \geq 5$*, with* $\mathbf{A}$ *defined in Eq. 7, the decomposition in Eqs. (8, 9, 10) always succeeds and yields four distinct solutions. If rank*$(\mathbf{A}) < 5$ *the solver returns infinitely many solutions.*

Proof: First assume rank$(\mathbf{A}) \geq 5$. Then SVD returns two distinct principle directions $\pm\hat{\mathbf{x}}$. After decomposition, Eq. 10 yields two more solutions, resulting in a total of four distinct solutions. Now assume that the decomposition fails, and this can happen for three reasons:

Failure to normalize in Eq. 8: Normalization may fail if $\hat{\mathbf{x}}_{4:6}$ has zero norm. However, this case is impossible for a matrix $\mathbf{A}$ with rank ≥ 5 for the following reason: Let $\mathbf{B}, \mathbf{C}$ be the three left and right columns of $\mathbf{A}$ (see Eq. 7). Moreover, note that $\mathbf{C} = \mathbf{TB}$, where $\mathbf{T} = \text{diag}(t'_1, t'_2, ..., t'_N)$ is a diagonal matrix, *i.e*. each row of $\mathbf{B}$ is a multiple of the corresponding row in $\mathbf{C}$.

If $\hat{\mathbf{x}}_{4:6}$ has zero norm, $\hat{\mathbf{x}}_{4:6} = 0$. Next, let σ be the smallest singular value of $\mathbf{A}$ corresponding to the solution $\hat{\mathbf{x}}$. Then

$$\mathbf{A}^\intercal\mathbf{A}\hat{\mathbf{x}} = \sigma\hat{\mathbf{x}} \tag{15}$$

$$\begin{bmatrix}\mathbf{B}^\intercal \\ \mathbf{B}^\intercal\mathbf{T}\end{bmatrix}\begin{bmatrix}\mathbf{B} & \mathbf{TB}\end{bmatrix}\begin{bmatrix}\hat{\mathbf{x}}_{1:3} \\ 0\end{bmatrix} = \begin{bmatrix}\sigma\hat{\mathbf{x}}_{1:3} \\ 0\end{bmatrix} \tag{16}$$

$$\begin{bmatrix}\mathbf{B}^\intercal\mathbf{B}\hat{\mathbf{x}}_{1:3} \\ \mathbf{B}^\intercal\mathbf{TB}\hat{\mathbf{x}}_{1:3}\end{bmatrix} = \begin{bmatrix}\sigma\hat{\mathbf{x}}_{1:3} \\ 0\end{bmatrix} \tag{17}$$

The last three rows of the last equation are

$$\mathbf{B}^\intercal\mathbf{TB}\hat{\mathbf{x}}_{1:3} = 0\,, \tag{18}$$

and imply either that $\mathbf{B}^\intercal(\mathbf{TB}\hat{\mathbf{x}}_{1:3}) = 0$, *i.e*. $\mathbf{TB}\hat{\mathbf{x}}_{1:3}$ is in the left null-space of $\mathbf{B}$, or $\mathbf{B}\hat{\mathbf{x}}_{1:3} = 0$, *i.e*. $\hat{\mathbf{x}}_{1:3}$ is in the right null-space of $\mathbf{B}$. Both imply that rank$(\mathbf{B}) < 3$. This can only be the case if rank$(\mathbf{A}) = 5$, following the assumption. This implies that the smallest singular value is $\sigma = 0$. From the first three equations above, this implies that $\mathbf{B}\hat{\mathbf{x}}_{1:3} = 0$. But then

$$\mathbf{A}\begin{bmatrix}0 \\ \mathbf{x}_{1:3}\end{bmatrix} = \mathbf{TB}\mathbf{x}_{1:3} = 0\,, \tag{19}$$

which implies that $\hat{\mathbf{x}} = [0^\intercal\ \mathbf{x}_{1:3}^\intercal]$ is also in the null space of $\mathbf{A}$. We now find that both $\hat{\mathbf{x}}_1 = [0^\intercal\ \mathbf{x}_{1:3}^\intercal]$ and $\hat{\mathbf{x}}_2 = [\mathbf{x}_{1:3}^\intercal\ 0^\intercal]$ are in the null-space of $\mathbf{A}$. These vectors are independent, and render the rank of $\mathbf{A} < 5$. This is a contradiction.

Failure to recover $\mathbf{e}_1^\ell$*:* Recovering $\mathbf{e}_1^\ell$ fails if the norm of the cross product in Eq. 10 is 0. This implies that $\hat{\mathbf{x}}_{4:6} = \lambda\hat{\mathbf{x}}_{1:3}$. For similar reasons as above, this implies that $\hat{\mathbf{x}}_{1:3}$ solves both $\mathbf{Bx} = 0$ and $\mathbf{Cx} = 0$. This implies that λ can be freely varied, which would imply a two-dimensional null space of $\mathbf{A}$ and a rank ≤ 4 which is again a contradiction.

Line passing through the origin at $t' = 0$*:* Note that in such a case, $\mathbf{e}_3^\ell$ would not be defined, and could cause issues in solving. However, we can then use a different definition of the line, with the direction $\mathbf{d} = \mathbf{e}_1^\ell$, and point on the line $\mathbf{P} = \mathbf{e}_1^\ell$. The line moment then becomes $\mathbf{m} = \mathbf{P} \times \mathbf{d} = 0$. Inserting this into Eq. 2, transforms Eq. 6 into

$$\mathbf{f}_j'^\intercal(\mathbf{e}_3^\ell u_y^\ell - \mathbf{e}_2^\ell u_z^\ell) = 0\,. \tag{20}$$

However, this would imply that the system in Eq. 7 has a solution of the form $\hat{\mathbf{x}} = [\hat{\mathbf{x}}_{1:3}^\intercal\ \mathbf{0}^\intercal]^\intercal$, with $\hat{\mathbf{x}}_{1:3} = \mathbf{e}_3^\ell u_y^\ell - \mathbf{e}_2^\ell u_z^\ell$. However, we proved in the last two cases that such a solution form implies that the rank of $\mathbf{A}$ is smaller than 5.

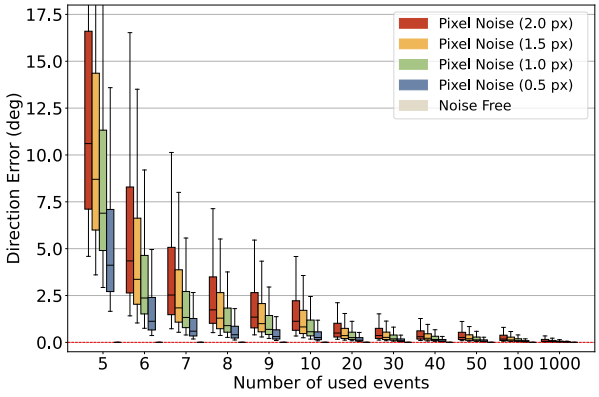

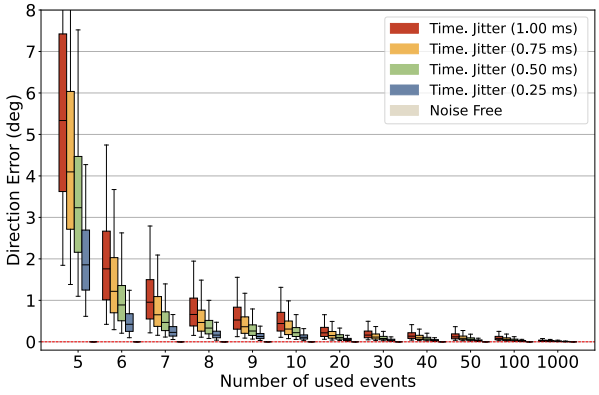

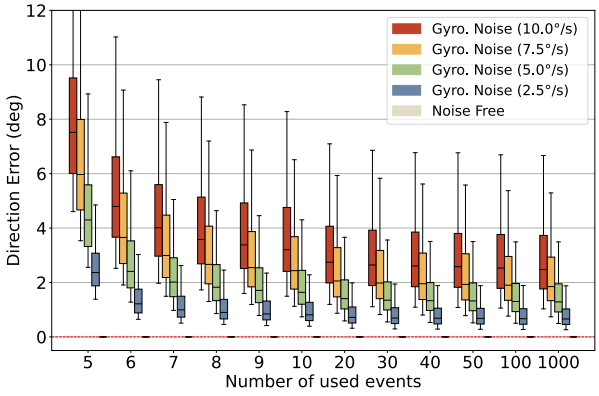

Figure 5. Analysis of the number of used events over three types of representative noise, *i.e*. pixel noise, timestamp jitter, and gyroscope noise.

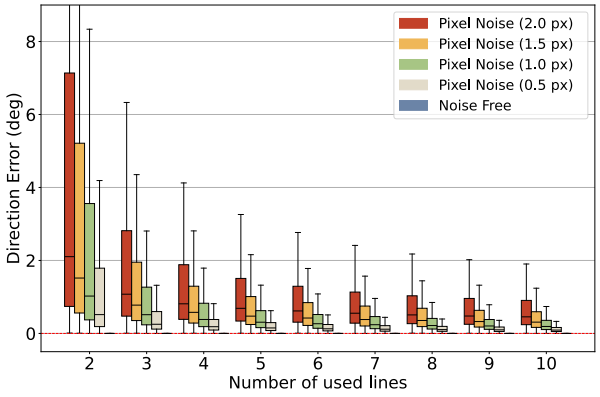

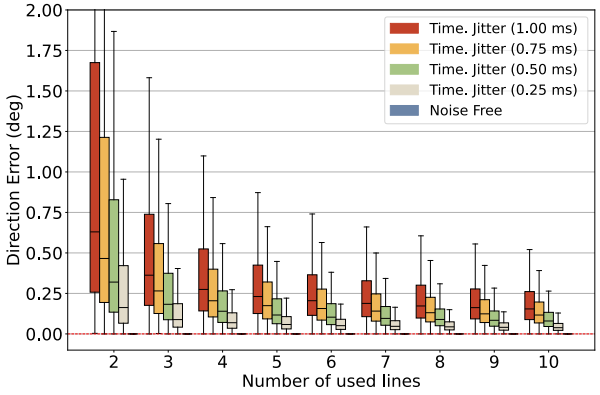

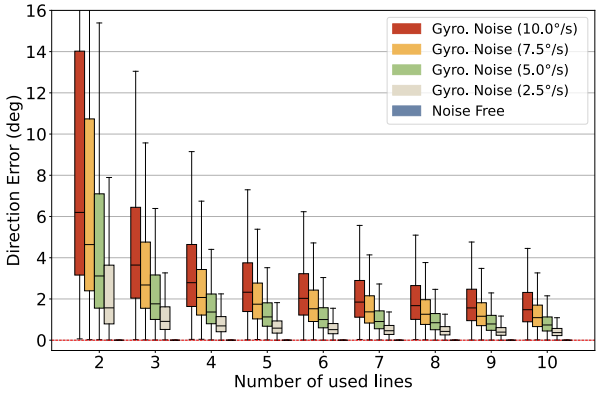

Figure 6. Analysis of the number of used lines over three types of representative noise, *i.e*. pixel noise, timestamp jitter, and gyroscope noise.

Thus ensuring $\text{rank}(\mathbf{A}) \geq 5$ is sufficient for discarding the case where the line passes through the origin.

We conclude that if $\text{rank}(\mathbf{A}) \geq 5$, the decomposition cannot fail, and always returns four distinct solutions. Moreover, we conclude that a $\text{rank}(\mathbf{A}) < 5$ yields solutions $\hat{\mathbf{x}}$ from a two dimensional nullspace, which yields infinitely many decompositions. ■

7.3. Proof of Theorem 2 on Solution Multiplicity

For clarity, we restate Theorem 2 here:

Theorem 2: *Given a solution* $S_0 = \{\mathbf{e}_1^\ell, \mathbf{e}_2^\ell, \mathbf{e}_3^\ell, u_y^\ell, u_z^\ell\}$ *to the incidence relation in Eq. 6, then*

$$
\begin{aligned}
S_1 &= \{\mathbf{e}_1^\ell, -\mathbf{e}_2^\ell, -\mathbf{e}_3^\ell, u_y^\ell, u_z^\ell\}\,, \\
S_2 &= \{-\mathbf{e}_1^\ell, \mathbf{e}_2^\ell, -\mathbf{e}_3^\ell, -u_y^\ell, u_z^\ell\}\,, \\
S_3 &= \{-\mathbf{e}_1^\ell, -\mathbf{e}_2^\ell, \mathbf{e}_3^\ell, -u_y^\ell, u_z^\ell\}
\end{aligned}
$$

are also solutions. These four solutions are visualized in Fig. 2. For solutions S_1 and S_2 the closest point $-\mathbf{e}_3^\ell$ on the line is behind the camera, while for solutions S_2 and S_3 the line direction $\mathbf{e}_1^\ell$ is flipped, which represents an ambiguity in the definition of direction of $\mathbf{L}$.

Proof: We will only prove solutions S_1 and S_2 since S_3 can be derived from a composition of S_1 and S_2. Inserting $S_1 = \{\mathbf{e}_1^{\ell\prime}, \mathbf{e}_2^{\ell\prime}, \mathbf{e}_3^{\ell\prime}, u_y^{\ell\prime}, u_z^{\ell\prime}\} = \{\mathbf{e}_1^\ell, -\mathbf{e}_2^\ell, -\mathbf{e}_3^\ell, u_y^\ell, u_z^\ell\}$ into Eq. 6, we have

$$\begin{aligned} & t_j' \mathbf{f}_j'^\intercal (u_z^{\ell\prime} \mathbf{e}_2^{\ell\prime} - u_y^{\ell\prime} \mathbf{e}_3^{\ell\prime}) + \mathbf{f}_j'^\intercal \mathbf{e}_2^{\ell\prime} \\ = \; & t_j' \mathbf{f}_j'^\intercal (u_z^\ell (-\mathbf{e}_2^\ell) - u_y^\ell (-\mathbf{e}_3^\ell)) + \mathbf{f}_j'^\intercal (-\mathbf{e}_2^\ell) \\ = \; & -(t_j' \mathbf{f}_j'^\intercal (u_z^\ell \mathbf{e}_2^\ell - u_y^\ell \mathbf{e}_3^\ell) + \mathbf{f}_j'^\intercal \mathbf{e}_2^\ell) \\ = \; & 0 \end{aligned}$$

and $S_2 = \{\mathbf{e}_1^{\ell\prime\prime}, \mathbf{e}_2^{\ell\prime\prime}, \mathbf{e}_3^{\ell\prime\prime}, u_y^{\ell\prime\prime}, u_z^{\ell\prime\prime}\} = \{-\mathbf{e}_1^\ell, \mathbf{e}_2^\ell, -\mathbf{e}_3^\ell, -u_y^\ell, u_z^\ell\}$ yields

$$\begin{aligned} & t_j' \mathbf{f}_j'^\intercal (u_z^{\ell\prime\prime} \mathbf{e}_2^{\ell\prime\prime} - u_y^{\ell\prime\prime} \mathbf{e}_3^{\ell\prime\prime}) + \mathbf{f}_j'^\intercal \mathbf{e}_2^{\ell\prime\prime} \\ = \; & t_j' \mathbf{f}_j'^\intercal (u_z^\ell \mathbf{e}_2^\ell - (-u_y^\ell)(-\mathbf{e}_3^\ell)) + \mathbf{f}_j'^\intercal \mathbf{e}_2^\ell \\ = \; & t_j' \mathbf{f}_j'^\intercal (u_z^\ell \mathbf{e}_2^\ell - u_y^\ell \mathbf{e}_3^\ell) + \mathbf{f}_j'^\intercal \mathbf{e}_2^\ell \\ = \; & 0 \end{aligned}$$

■

7.4. Handling of Parallel Lines

As mentioned in the main text, parallel lines may cause difficulties in identifying the $\mathbf{e}_1^\ell$ direction of the camera velocity. However, we can identify this case easily by checking the rank of $\mathbf{D}$. If it is lower than 2, we can discard the sample, and select a new one, or even use another RANSAC loop to select pairs of lines until the rank of $\mathbf{D}$ is at least 2. Let us now prove that parallel lines cause a rank deficiency in $\mathbf{D}$.

Proof: We will proceed in showing that if two lines are parallel, the two corresponding rows $\mathbf{r}_1 = u_{y1}^\ell \mathbf{e}_{31}^\ell - u_{z1}^\ell \mathbf{e}_{21}^\ell$ and $\mathbf{r}_2 = u_{y2}^\ell \mathbf{e}_{32}^\ell - u_{z2}^\ell \mathbf{e}_{22}^\ell$ in $\mathbf{D}$ are parallel and will thus result in rank deficiency (see Eq. 13). Expanding $\mathbf{v}$ in the two line coordinate frames yields

$$\lambda_1 \mathbf{v} = u_{x1}^\ell \mathbf{e}_{11}^\ell + u_{y1}^\ell \mathbf{e}_{21}^\ell + u_{z1}^\ell \mathbf{e}_{31}^\ell \tag{21}$$

$$\lambda_2 \mathbf{v} = u_{x2}^\ell \mathbf{e}_{12}^\ell + u_{y2}^\ell \mathbf{e}_{22}^\ell + u_{z2}^\ell \mathbf{e}_{32}^\ell \tag{22}$$

with unknown scale factors λ_1, λ_2. For parallel lines $\mathbf{e}_{11}^\ell = \mathbf{e}_{12}^\ell \doteq \mathbf{e}_1^\ell$. Computing $\mathbf{e}_1^\ell \times \mathbf{v}$ in two ways (with two expansions of $\mathbf{v}$), we recover exactly the rows of $\mathbf{D}$ by

$$\lambda_1 (\mathbf{e}_1^\ell \times \mathbf{v}) = u_{y1}^\ell \mathbf{e}_{31}^\ell - u_{z1}^\ell \mathbf{e}_{21}^\ell = \mathbf{r}_1 \tag{23}$$

$$\lambda_2 (\mathbf{e}_1^\ell \times \mathbf{v}) = u_{y2}^\ell \mathbf{e}_{32}^\ell - u_{z2}^\ell \mathbf{e}_{22}^\ell = \mathbf{r}_2 \tag{24}$$

It follows that $\mathbf{r}_1 = \frac{\lambda_1}{\lambda_2} \mathbf{r}_2$, *i.e.* they are parallel. ■

7.5. Global Optimality of $\mathbf{R}_l$ and $\mathbf{u}_l$

As noted in the main text, while the SVD-based solver which recovers $\hat{\mathbf{x}}$ from a set of incidence relations (Eq. 7) finds a globally optimal solution $\hat{\mathbf{x}}$, it is not clear if the decomposed solution $\mathbf{R}_l, \mathbf{u}_l$ is also optimal with respect to the same objective. We prove this here.

Proof: We will prove this by way of contradiction. Assume given the SVD-based solution

$$\hat{\mathbf{x}} = \arg\min_{\mathbf{x}} \|\mathbf{A}\mathbf{x}\|^2 \quad \text{such that} \quad \|\mathbf{x}\|^2 = 1.$$

which is globally optimal, and decomposition $\mathbf{R}_l, \mathbf{u}_l$ with $\hat{\mathbf{x}} = \mathbf{x}(\mathbf{R}_l, \mathbf{u}_l)$. Assume that there exists a different, more optimal $\mathbf{R}_l', \mathbf{u}_l'$ with $\hat{\mathbf{x}}' = \mathbf{x}(\mathbf{R}_l', \mathbf{u}_l')$. Then $\|\mathbf{A}\hat{\mathbf{x}}'\|^2 < \|\mathbf{A}\hat{\mathbf{x}}\|^2$ but this is impossible since it would imply that $\hat{\mathbf{x}}'$ is more optimal than $\hat{\mathbf{x}}$, but $\hat{\mathbf{x}}$ is already optimal. This implies that the objective is already optimal in $\mathbf{R}_l, \mathbf{u}_l$ which concludes the proof. ■

7.6. Connection between the Proposed Line Averaging Scheme and [12]

The presented velocity averaging scheme is conceptually simpler, and lends itself to geometric interpretation, unlike the scheme in [12]. However, surprisingly these schemes are actually equivalent, as will be demonstrated next. In [12], Eq. 11 is used to set up a number of constraints

$$\mathbf{e}_{2i}^{\ell\,\intercal} \mathbf{v} - \lambda_i u_{yi}^\ell = 0 \tag{25}$$

$$\mathbf{e}_{3i}^{\ell\,\intercal} \mathbf{v} - \lambda_i u_{zi}^\ell = 0 \tag{26}$$

Introducing unknowns $\mathbf{v}$ and $\{\lambda_i\}$, one for each line. Stacking multiple of these equations results in a system

$$\underbrace{\begin{bmatrix} \mathbf{e}_{21}^{\ell\,\intercal} & -u_{y1}^\ell & \cdots & 0 \\ \mathbf{e}_{31}^{\ell\,\intercal} & -u_{z1}^\ell & \cdots & 0 \\ \vdots & \ddots & \ddots & \vdots \\ \mathbf{e}_{2M}^{\ell\,\intercal} & 0 & \cdots & -u_{yM}^\ell \\ \mathbf{e}_{3M}^{\ell\,\intercal} & 0 & \cdots & -u_{zM}^\ell \end{bmatrix}}_{\mathbf{E}} \begin{bmatrix} \mathbf{v} \\ \lambda_1 \\ \vdots \\ \lambda_M \end{bmatrix} = \mathbf{0}\,. \tag{27}$$

This system is then multiplied from the left with $\mathbf{E}^\intercal$, and the Shur complement trick is employed to eliminate the extraneous variables λ_i, resulting in the equation $\mathbf{F}\mathbf{v} = \mathbf{0}$,

where we use the following definitions:

$$\mathbf{F} = \mathbf{U} - \mathbf{W}\mathbf{V}^{-1}\mathbf{W}^\intercal \tag{28}$$

$$\mathbf{U} = \sum_{i=1}^{M} (\mathbf{e}_{2i}^{\ell}\mathbf{e}_{2i}^{\ell\,\intercal} + \mathbf{e}_{3i}^{\ell}\mathbf{e}_{3i}^{\ell\,\intercal}) \tag{29}$$

$$\mathbf{V} = \operatorname{diag}\left(u_{y1}^{\ell\,2} + u_{z1}^{\ell\,2}, \cdots, u_{yM}^{\ell\,2} + u_{zM}^{\ell\,2}\right) \tag{30}$$

$$\mathbf{W}^\intercal = \begin{bmatrix} -u_{y1}^{\ell}\mathbf{e}_{21}^{\ell\,\intercal} - u_{z1}^{\ell}\mathbf{e}_{31}^{\ell\,\intercal} \\ \vdots \\ -u_{yM}^{\ell}\mathbf{e}_{2M}^{\ell\,\intercal} - u_{zM}^{\ell}\mathbf{e}_{3M}^{\ell\,\intercal} \end{bmatrix} \tag{31}$$

Inserting the equations, and simplifying we get

$$\begin{aligned} \mathbf{F} =& \sum_{i=1}^{M} (\mathbf{e}_{2i}^{\ell}\mathbf{e}_{2i}^{\ell\,\intercal} + \mathbf{e}_{3i}^{\ell}\mathbf{e}_{3i}^{\ell\,\intercal}) \\ & - \frac{\left(-u_{yi}^{\ell}\mathbf{e}_{2i}^{\ell} - u_{zi}^{\ell}\mathbf{e}_{3i}^{\ell}\right)\left(-u_{yi}^{\ell}\mathbf{e}_{2i}^{\ell\,\intercal} - u_{zi}^{\ell}\mathbf{e}_{3i}^{\ell\,\intercal}\right)}{u_{yi}^{\ell\,2} + u_{zi}^{\ell\,2}} \qquad (32) \\ =& \sum_{i=1}^{M} \frac{1}{u_{yi}^{\ell\,2} + u_{zi}^{\ell\,2}} \left(u_{zi}^{\ell\,2}\mathbf{e}_{2i}^{\ell}\mathbf{e}_{2i}^{\ell\,\intercal} + u_{yi}^{\ell\,2}\mathbf{e}_{3i}^{\ell}\mathbf{e}_{3i}^{\ell\,\intercal}\right. \\ & \left. - u_{yi}^{\ell}u_{zi}^{\ell}\mathbf{e}_{3i}^{\ell}\mathbf{e}_{2i}^{\ell\,\intercal} - u_{yi}^{\ell}u_{zi}^{\ell}\mathbf{e}_{2i}^{\ell}\mathbf{e}_{3i}^{\ell\,\intercal}\right) \qquad (33) \\ =& \sum_{i=1}^{M} \frac{\left(u_{yi}^{\ell}\mathbf{e}_{3i}^{\ell} - u_{zi}^{\ell}\mathbf{e}_{2i}^{\ell}\right)\left(u_{yi}^{\ell}\mathbf{e}_{3i}^{\ell} - u_{zi}^{\ell}\mathbf{e}_{2i}^{\ell}\right)^\intercal}{u_{zi}^{\ell\,2} + u_{zi}^{\ell\,2}} \qquad (34) \\ =& \hat{\mathbf{D}}^\intercal\hat{\mathbf{D}} \qquad (35) \end{aligned}$$

with

$$\hat{\mathbf{D}} = \begin{bmatrix} \frac{1}{\sqrt{u_{y1}^{\ell\,2} + u_{z1}^{\ell\,2}}}\left(u_{y1}^{\ell}\mathbf{e}_{31}^{\ell} - u_{z1}^{\ell}\mathbf{e}_{21}^{\ell}\right) \\ \vdots \\ \frac{1}{\sqrt{u_{yM}^{\ell\,2} + u_{zM}^{\ell\,2}}}\left(u_{yM}^{\ell}\mathbf{e}_{3M}^{\ell} - u_{zM}^{\ell}\mathbf{e}_{2M}^{\ell}\right) \end{bmatrix} \tag{36}$$

The linear system thus becomes

$$\mathbf{F}\mathbf{v} = \mathbf{0} \tag{37}$$

$$\hat{\mathbf{D}}^\intercal\hat{\mathbf{D}}\mathbf{v} = \mathbf{0} \tag{38}$$

$$\hat{\mathbf{D}}^\intercal(\hat{\mathbf{D}}\mathbf{v}) = \mathbf{0} \tag{39}$$

if $\hat{\mathbf{D}}^\intercal$ has full rank this implies that

$$\hat{\mathbf{D}}\mathbf{v} = \mathbf{0} \tag{40}$$

Note that $\hat{\mathbf{D}}$ is identical to $\mathbf{D}$ in Eq. 13 up to normalization of each velocity $\mathbf{u}_i^\ell$ separately. This normalization strategy can be seamlessly integrated into the computation of $\mathbf{D}$. Moreover, computing $\mathbf{D}$ is much simpler than computing $\mathbf{F}$.

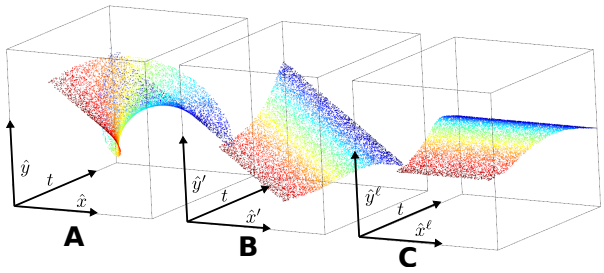

(i) event transformations

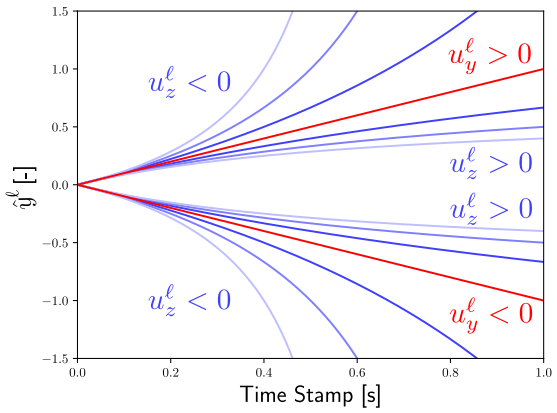

(ii) eventail in 2D

Figure 7. Events triggered by a line observed by an event camera span a non-linear manifold called *éventail* (A). We show that this manifold imposes a linear constraint on the partial camera velocity and line parameters. With this insight, we can design a linear solver for these quantities that is both fast and highly interpretable, and characterize all manifolds (A) by transforming them into canonical form via rotation compensation (B), and transformation into the line coordinate frame (C). In the $\hat{y}^\ell t$-plane, these manifolds trace a family of curves (ii), depending on the configuration of u_z^ℓ and u_y^ℓ.

7.7. Canonicalization of the Manifold

The incidence relation in Eq. 6 yields a simple way to visualize the manifold in its canonical form, and also shows the dependence on the line velocity parameters u_y^ℓ and u_z^ℓ. To reach this canonical form, we simply rotate the bearing vectors of all events into the line-dependent coordinate frame by replacing $\mathbf{f}' = \mathbf{R}_\ell\hat{\mathbf{f}}'$. We visualize this transformation in Fig. 7, where we transition from raw events in normalized coordinates (A), derotated events (B), and then events in the line reference frame (C). This coordinate frame corresponds with that of a line that is parallel to the camera's x-axis. Doing this replacement yields

$$t'\hat{\mathbf{f}}_j'^\intercal(u_z^\ell\mathbf{e}_y - u_y^\ell\mathbf{e}_z) + \hat{\mathbf{f}}_j'^\intercal\mathbf{e}_y = 0\,, \tag{41}$$

where $\mathbf{e}_{x/y/z}$ corresponds to the unit vectors in the camera coordinate frame. Distributing and diving out the third component of $\hat{\mathbf{f}}_j'$, *i.e.* transitioning to normalized coordinates in

the new line reference frame, we reach

$$0 = t'(u_z^\ell \hat{y}^\ell - u_y^\ell) + \hat{y}^\ell \implies \hat{y}^\ell = \frac{u_y^\ell t'}{1 + u_z^\ell t'} \quad (42)$$

where $\hat{y}^\ell$ is the event y-coordinate in normalized, line coordinates. This form describes the shape of the manifold in two dimensions and is visualized in Fig. 7(ii) for varying u_y^ℓ and u_z^ℓ.

From these visualization we make a number of observations: First, configurations with $u_z^\ell = 0$ trace straight lines, corresponding to planar manifolds in the line coordinate frame. Note, however, that in the derotated frame (B) these may still be non-planar. Second, we see that $u_z^\ell < 0$ induces a curvature in the manifold which increases as time progresses. This configuration corresponds to a camera approaching the line, and thus the reduced distance increases the apparent motion, which results in a larger slope. Finally, $u_z^\ell > 0$ results in flattened curves. This corresponds to cameras retracting from the line, which reduces the apparent motion, and thus reduces the slope in the manifold.